AGU ADVANCING EARTH AND SPACE SCIENCE

JGR Space Physics

RESEARCH ARTICLE
10.1029/2020JA028503

Key Points:

- A radiation belt electron dropout was observed during injection-associated electromagnetic ion cyclotron (EMIC) waves
- L-shell and energy-dependent electron dropout indicates EMIC-wave induced scattering of radiation belt electrons
- NOAA spacecraft data show relativistic electron precipitation during the dropout event

Correspondence to:
H. Kim,
hmkim@njit.edu

Citation:
Kim, H., Schiller, Q., Engebretson, M. J., Noh, S., Kuzichev, I., Lanzerotti, L. J., et al. (2021). Observations of particle loss due to injection-associated electromagnetic ion cyclotron waves. *Journal of Geophysical Research: Space Physics*, *126*, e2020JA028503. https://doi.org/10.1029/2020JA028503

Received 18 JUL 2020
Accepted 25 NOV 2020

Observations of Particle Loss due to Injection-Associated Electromagnetic Ion Cyclotron Waves

Hyomin Kim[1], Quintin Schiller[2], Mark J. Engebretson[3], Sungjun Noh[1], Ilya Kuzichev[1,4], Louis J. Lanzerotti[1], Andrew J. Gerrard[1], Khan-Hyuk Kim[5], Marc R. Lessard[6], Harlan E. Spence[6], Dae-Young Lee[7], Jürgen Matzka[8], and Tanja Fromm[9]

[1]New Jersey Institute of Technology, Newark, NJ, USA, [2]Space Science Institute, Boulder, CO, USA, [3]Augsburg University, Minneapolis, MN, USA, [4]Space Research Institute of RAS, Moscow, Russia, [5]Kyung Hee University, Yongin, Republic of Korea, [6]University of New Hampshire, Durham, NH, USA, [7]Chungbuk National University, Cheongju, Republic of Korea, [8]GFZ German Research Centre for Geosciences, Potsdam, Germany, [9]Alfred-Wegener Institute, Bremerhaven, Germany

Abstract We report on observations of electromagnetic ion cyclotron (EMIC) waves and their interactions with injected ring current particles and high energy radiation belt electrons. The magnetic field experiment aboard the twin Van Allen Probes spacecraft measured EMIC waves near $L = 5.5$–6. Particle data from the spacecraft show that the waves were associated with particle injections. The wave activity was also observed by a ground-based magnetometer near the spacecraft geomagnetic footprint over a more extensive temporal range. Phase space density profiles, calculated from directional differential electron flux data from Van Allen Probes, show that there was a significant energy-dependent relativistic electron dropout over a limited L-shell range during and after the EMIC wave activity. In addition, the NOAA spacecraft observed relativistic electron precipitation associated with the EMIC waves near the footprint of the Van Allen Probes spacecraft. The observations suggest EMIC wave-induced relativistic electron loss in the radiation belt.

Plain Language Summary Electromagnetic waves caused by plasma particles in the Earth's magnetic fields are known to interact with high energy particles in the Earth's radiation belts, leading to loss of the particles into the Earth's atmosphere. We report on observations of the wave phenomena and their interaction with radiation belt particles using data from NASA's twin spacecraft mission called Van Allen Probes. Particle detectors aboard the spacecraft measured the increased flux of particles, providing the source energy to generate electromagnetic waves. Such wave activity was also observed by instruments on the ground. A parameter calculated using data from various instruments aboard the spacecraft enabled us to quantitatively assess how the radiation belt electron population changes over time. This analysis reveals that the wave event caused the radiation belt electrons of certain energies to decay over a limited spatial extent. In addition, particle data from low earth orbiting spacecraft show an increase in particle flux, which appears to be associated with the wave activity. The observations suggest that the wave can contribute to loss of electrons in the radiation belts.

1. Introduction

Electromagnetic ion cyclotron (EMIC) waves are known to be generated by the cyclotron instability of anisotropic distributions of medium energy ring current and plasmasheet protons in the equatorial region of the magnetosphere in the energy range of a few to hundreds of kilo-electronvolts during geomagnetic storms and substorms (Anderson et al., 1996; Clausen et al., 2011; Erlandson & Ukhorskiy, 2001; Fraser et al., 2010; Halford et al., 2010; Jordanova et al., 2001; Keika et al., 2013; Kennel & Petschek, 1966; Kozyra et al., 2013; Lin et al., 2014; Lyons & Thorne, 1972; Noh et al., 2018; Summers & Thorne, 2003; Thorne, 2010; Thorne & Kennel, 1971; Zhang et al., 2016). Magnetospheric compression due to solar wind dynamic pressure increases has also been considered to be one of the generation mechanisms for EMIC waves (Anderson & Hamilton, 1993; Anderson et al., 1992; Cho et al., 2016; Engebretson et al., 2002, 2015; H. Kim et al., 2017; Lessard et al., 2019; Park et al., 2016; Saikin et al., 2016; Usanova et al., 2012, 2010). While occurrences of EMIC waves increase typically in the aftermath of geomagnetic storms or during the main phase of such storms, EMIC waves during quiet times and/or storm recovery phases have also been reported (Clausen et al., 2011; Halford et al., 2010, 2015; K.-H. Kim et al., 2016; Saikin et al., 2016; Usanova et al., 2008).

Radial and local time occurrences of EMIC waves in the magnetosphere appear to be widely distributed: preferentially observed at $L > 7$ at 11–15 MLT (Allen et al., 2015; Anderson et al., 1992; Usanova et al., 2012); in the inner magnetosphere (near $L = 6$) in the afternoon section (Halford et al., 2010; Saikin et al., 2015), at $L = 10$–12 in the dawnside for H+ band waves and at $L = 8$–12 in the duskside for He + band waves (Min et al., 2012), at $L > 7$ in the afternoon sector for H+ band waves and at $L < 6$ near the afternoon to dusk sector for He + band (Keika et al., 2013; Saikin et al., 2015). The prenoon sector has also been found to be a favorable location in the inner magnetosphere (Saikin et al., 2015). A number of studies have shown that EMIC waves are observed preferentially in the inner magnetosphere near the storm-time plume (e.g., L. Chen et al., 2009; Clausen et al., 2011; Erlandson & Ukhorskiy, 2001; Halford et al., 2010; Keika et al., 2013). In addition, there is recent studies showing that wave occurrences are not strongly correlated with the plasmapause location (e.g., Tetrick et al., 2017).

As mentioned above, substorms are known to be one of the major sources for EMIC wave generation. Historically, there have been a number of reports on "intervals of pulsations with diminishing periods (IPDP)," a subset of EMIC waves which are known to be associated with substorm activity (Arnoldy et al., 1979; Hayashi et al., 1988; Kangas et al., 1987; Søraas et al., 1980; Yahnina et al., 2003), followed by more recent studies suggesting plasmaspheric plumes as a favorable location of EMIC wave enhancements in association with ring current injections (Halford et al., 2015; Morley et al., 2009; Spasojević et al., 2004; Yuan et al., 2010). Direct evidence of injection-associated EMIC wave events has also been reported (L. W. Blum et al., 2015; Remya et al., 2018, 2020).

One of the important aspects of EMIC waves is their important role in pitch-angle scattering relativistic electrons in the outer radiation belt via cyclotron resonant interactions, thus leading to the precipitation of both tens of kilo-electronvolts ions and million electronvolts electrons to the ionosphere (e.g., Albert & Bortnik, 2009; Denton et al., 2019; Engebretson et al., 2015; Jordanova et al., 2008; Khazanov & Gamayunov, 2007; L. Blum et al., 2019; L. W. Blum et al., 2020; Lee et al., 2020; Lessard et al., 2019; Loto'aniu et al., 2006; Meredith et al., 2003; Miyoshi et al., 2008; Qin et al., 2018; Qin et al., 2020; Thorne, 2010; Ukhorskiy et al., 2010; Usanova et al., 2014; Z. Li et al., 2014). The radiation belt electron dropout in association with EMIC waves has been shown as decreases in phase space density (PSD) (e.g., Engebretson et al., 2015, 2018; Shprits et al., 2016; Turner et al., 2014; Xiang et al., 2017; Zhang et al., 2016). Scattering loss of electrons with energies of a few MeV due to EMIC waves can be very efficient with the time scale of minutes (e.g., Thorne & Kennel, 1971) and even seconds (Ukhorskiy et al., 2010).

Although there have been a number of theoretical studies showing efficient scattering of radiation belt electrons by EMIC waves as listed above, systematic observations to support such an effect have not been extensively reported. It is still challenging to observe a direct relationship between EMIC waves and corresponding electron dropout and precipitation, though some studies have shown limited success (e.g., Capannolo, Li, Ma, Chen, et al., 2019; Capannolo, Li, Ma, Shen, et al., 2019). This study reports a radiation belt dropout associated with EMIC waves that were observed by the Van Allen Probes spacecraft, direct evidence of such a correspondence which is still not frequently reported due to the limited in-situ observing capability.

2. Data Sets

The primary data used in this study were from the Van Allen Probes mission. For magnetic field observations, level-3, high time-resolution (64 Hz) data from the Electric and Magnetic Field Instruments Suite and Integrated Science (EMFISIS) instrument (Kletzing et al., 2013) were used. Proton flux data (level-3, pitch angle and pressure and spin-averaged [~11 s]) in the energy range of ~40–600 keV were acquired by the Radiation Belt Storm Probes Ion Composition Experiment (RBSPICE) instrument (Mitchell et al., 2013). Proton flux data (level-3 and spin-averaged) in the energy range of ~1 eV–50 keV were from the Helium Oxygen Proton Electron (HOPE) plasma spectrometer (Funsten et al., 2013) of the Energetic Particle, Composition, and Thermal Plasma Suite (ECT) (Spence et al., 2013).

Both DC and AC magnetic field data near the ground magnetic footprint of Van Allen Probes were acquired by the fluxgate and induction-coil magnetometers at Neumayer Station (VNA), Antarctica (Wesche et al., 2016). The fluxgate magnetometer at VNA provides tri-axial, 1-s resolution data. The induction-coil magnetometer, part of the Magnetic Induction-Coil Array (MICA) provides 20-Hz, bi-axial, time-varying magnetic field (dB/dt) data for wave observations. Solar wind parameters (IMF and dynamic pressure) were provided from high time-resolution (1 min) OMNI data (King & Papitashvili, 2005). For ring current and auroral electrojet activities, Applied Physics Laboratory (APL) SuperMAG indices (Gjerloev, 2012; Newell & Gjerloev, 2011, 2012) were used. Particle precipitation data were obtained by the Medium Energy Proton and Electron Detector (MEPED) aboard the NOAA Polar Orbiting Environmental Satellites (POES) (Galand & Evans, 2000), which monitors the intensities of protons and electrons at an altitude of ~800 km over a range extending from 30 keV to more than 200 MeV.

PSDs of electrons in adiabatic coordinates were calculated from the directional differential electron flux from both Magnetic Electron Ion Spectrometer (MagEIS) (Blake et al., 2013) and the Relativistic Electron Proton Telescope (REPT) (Baker et al., 2013) of ECT aboard the Van Allen Probes spacecraft. The first invariant (μ) is calculated for a given energy channel and pitch angle from observations. The second invariant (K) is calculated by estimating magnetic field intensity at the mirror point (B_m) for a given pitch angle. All data are level-3. The International Geomagnetic Reference Field (IGRF) and Tsyganenko (TS05) (Tsyganenko & Sitnov, 2005) models were used as an internal and external model, respectively, to estimate the second (K) and third (L^*) adiabatic invariants. Also, note that both the PSDs and energy channels were interpolated for given μ's and K's. The PSD calculation methods used in this study are based on those introduced in previous studies (e.g., Y. Chen et al., 2005; Onsager et al., 2004; Roederer, 2012).

3. Observations

This study presents Van Allen Probes observations of EMIC waves in association with dispersive particle injection events on February 27, 2019 when both Spacecraft A and B were near the afternoon/dusk sector. Spacecraft A observations of waves and ring current particle flux enhancement, which is seemingly related to injection, are shown in Figure 1a, in which EMIC waves were observed between 14:00 and 15:00 UT (top panel). Spacecraft B observed a similar wave event between 17:30 and 19:00 UT associated with particle injection (Figure 1b) approximately 3.5 h after Spacecraft A observed the preceding event (Figure 1a), passing a similar local time sector (17:00–18:00 MLT) over a limited L-shell range (~5.5–6.0). The gyrofrequency curves (the white traces in this figure) indicated that the waves are mainly in the He-band. Both events display a mix of left-hand and linear polarization (second panel). Similar wave events were observed by both spacecraft in the next orbit (plots not shown here), indicating the persistent nature of the wave activity. The enhancement of proton flux (seen as dispersive particle injection) was detected over the energy range of ~5–100 keV in HOPE and RBSPICE data as shown in the third and bottom panels in Figures 1a and 1b. The injection appeared at ~12: 30 UT (~16: 00 UT) at ~100 keV (RBSPICE) and tapered off at ~16 : 00 UT (~20 : 30 UT) at ~10 keV (HOPE) as observed by Spacecraft A (Spacecraft B). Given their temporal extent as shown in both energy spectra in Figures 1a and 1b, the injection persisted from 12:30 to 20:30 UT. The electron density derived from EMFISIS level-4 data (not shown here) presented no clear plasmapause boundary while it appears that the observations were made within the plasmapause, given the values of electron density data.

Simultaneous observations of the EMIC waves near the ground geomagnetic footprint of the spacecraft observations are shown in Figure 2, displaying FFT-spectrograms of bi-axial search-coil magnetometer data from Neumayer Station in Antarctica (GMLAT = −61.1°, GMLON = 42.3°, L = 4.3). The two red boxes (a) and (b) in Figure 2 denote the time ranges when Van Allen Probes A and B observed the EMIC wave events, respectively. Although not strong, there was a persistent spectral structure from ~13:00 UT to ~19:00 UT as shown in the spectra of this figure. The fluxgate magnetometer data (top panel), on the other hand, do not present any remarkable signatures during the events. Only the Spacecraft B pass during the second wave interval (17:30–19:00 UT) was relatively close to the geomagnetic location of the station (VNA) as shown in Figure 3. For example, at 18:00 UT, Spacecraft B was at GMLAT = −68.6°, GMLON = 65.9°, and L = 6. The map also shows the magnetic footprint of Spacecraft B from 14:00 to 15:00 UT during which Spacecraft A observed the first event (see Figure 1a). However, the waves observed by Spacecraft B were weak (figure not shown here).

It is well known that waves generated at limited latitudes are measured over a wide range of L's on the ground owing to propagation in the ionospheric waveguide (e.g., H. Kim et al., 2011). Nevertheless, the

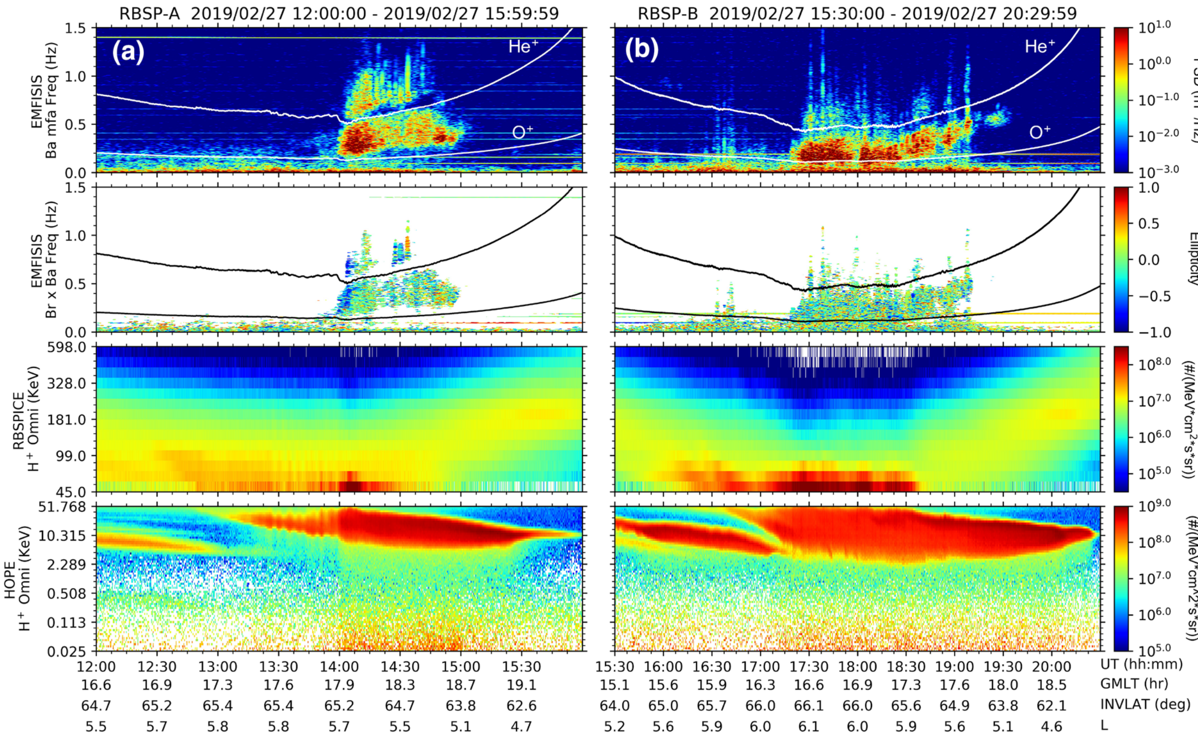

Figure 1. (a) Van Allen Probes-A Observations of EMIC waves and ring current particle injection: the spectra of the azimuthal component in mean field-aligned coordinates of EMFISIS data showing EMIC waves (top panel) and the wave polarization (second panel); RBSPICE (third panel) and HOPE (bottom panel) omni-flux data showing particle flux enhancement. (b) Same as (a) but for Van Allen Probes-B. The white traces indicate He^+ and O^+ gyrofrequencies. EMFISIS, Electric and Magnetic Field Instruments Suite and Integrated Science; EMIC, electromagnetic ion cyclotron; HOPE, Helium Oxygen Proton Electron; RBSPICE, Radiation Belt Storm Probes Ion Composition Experiment.

weak ground signature for Event (a) might be due to the longitudinal separation between the spacecraft and the ground station. The polarization at the ground for the first event (a) is linear although not strong and that for the second event (b) is right-handed and linear whereas a mix of left-hand and linear polarization was observed by Van Allen Probes (Figure 1). This polarization reversal (left-hand to right-hand) has been reported previously (Johnson & Cheng, 1999; E.-H. Kim & Johnson, 2016; Mann et al., 2014). The wave normal angles calculated using EMFISIS data (not shown here) are predominantly ≤ 20°, indicating that the wave propagation was mostly field-aligned.

Since the local noon at Neumayer is approximately 14:00 UT, the local time extent of the wave activity encompasses most of the postnoon sector (11–17 MLT) as observed from the ground data. Perhaps, the spacecraft observed only the “snapshot” of the long-lasting event. It appears that only the lower frequency component of the first event (a) was observed by the ground magnetometer while the spectral structure of the second event (b) remarkably resembles the space-borne counterpart. The second event (b), in particular, appears to be a classic substorm-associated IPDP event (in other words, rising spectral signatures), similar to the space-borne observations (Figure 1b). This is confirmed in Figure 4 in which large auroral electrojet indices were measured during the second event. The onset of the persistent Pc1 waves began at ∼13:00 UT also coincided with the large auroral electrojet indices presented in Figure 4 (refer to the next paragraph).

The solar wind parameters (IMF and dynamic pressure) from the OMNI data set and SuperMAG indices during the events are presented in Figure 4. The first event (Spacecraft A, ∼14:00–15:00 UT, red box [a]) occurred ∼30 min after the sudden decrease in solar wind dynamic pressure (Pdyn, second panel of the figure), followed by the second event (Spacecraft B, ∼17:30–19:00 UT, red box [b]) when the pressure remained stable (∼5 nPa). The IMF orientation was mostly northward with occasional southward turning occurred during the second event around 18:00 UT. The SuperMAG ring current index (SMR) was > -20 nT during the events (third panel of Figure 4), implying relatively quiet times. The first event occurred during a

10.1029/2020JA028503

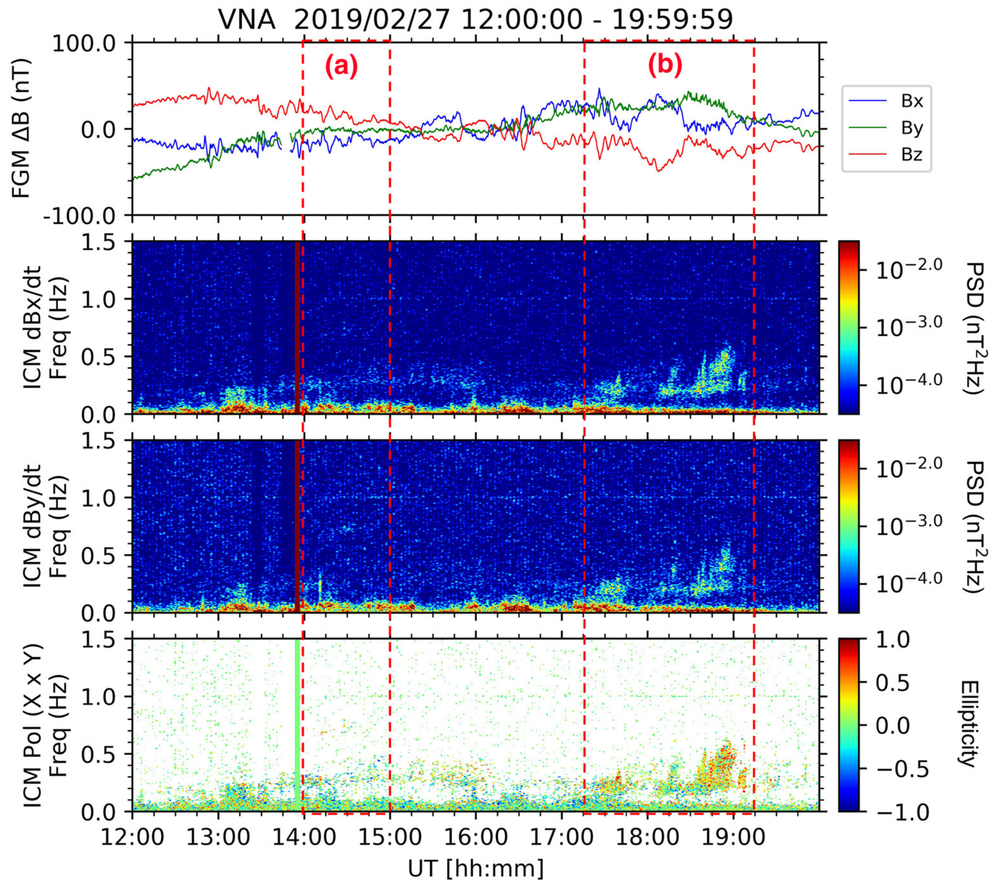

Figure 2. Magnetic field data from the fluxgate (top panel) and induction-coil magnetometers at Neumayer Station, Antarctica (VNA). Spectrograms of bi-axial induction-coil magnetometer data represent time-varying magnetic fields in the geomagnetic south (second panel) and geomagnetic east (third panel) components, both perpendicular to the local field. The wave polarization from the induction-coil magnetometer data is presented in the bottom panel. The first and second events observed by the Van Allen Probes spacecraft are indicated by the red rectangles (a) and (b), respectively. The local noon at Neumayer is approximately 14 UT.

descending period of auroral activity while the second event occurred during an interval of high auroral activity as indicated by the SuperMAG auroral electrojet indices or SME (fourth panel).

The temporal progression of PSDs and their distributions in L^*-values are demonstrated in Figure 5 which reveals that there were noticeable relativistic electron dropouts over $L^* = 4$–5 for lower energies (i.e., lower first adiabatic invariant, $\mu = 2000$ MeV/G) during and after the EMIC wave events (note the difference between black and red traces and between blue and light blue traces). At higher energies ($\mu = 4{,}000$ MeV/G), there was no clear dropout. Note that $\mu = 2{,}000$ MeV/G corresponds to ∼3.4 MeV at $L^* = 4$ and ∼2.4 MeV at $L^* = 5$ and $\mu = 4{,}000$ MeV/G corresponds to ∼5.0 MeV at $L^* = 4$ and ∼3.5 MeV at $L^* = 5$. PSDs at μ's corresponding to the higher energy ranges (∼3.5–5 MeV) using MagEIS and REPT data have been reliably estimated in a number of previous studies (e.g., Allison & Shprits, 2020; Foster et al., 2015; Katsavrias et al., 2019; Reeves et al., 2013). The maximum dropout occurred from the Spacecraft A observations at $L^* = 4.9$ for $\mu = 2000$ MeV/G and $K = 0.15\ R_E G^{1/2}$ (see the bottom left panel in Figure 5), for which the PSD change from 11:28:47 UT to 14:53:03 UT was −1.45e-9 (s^3/m^6). If the exponential fitting of the decay is used (e.g., Borovsky & Denton, 2009), this corresponds to a decay rate represented by e-folding time of ∼3.3 h. For $\mu = 4{,}000$ MeV/G (and the same K, see the bottom right panel in Figure 5), the maximum dropout occurred from the Spacecraft A observations at $L^* = 4.4$, for which the PSD change from 10:51:42 UT to 15:31:11 UT was −3.68e-11 (s^3/m^6), yielding the e-folding time of exponential decay ∼8 h. We note that the decay rates are approximate, as it is unknown when the PSD started to change.

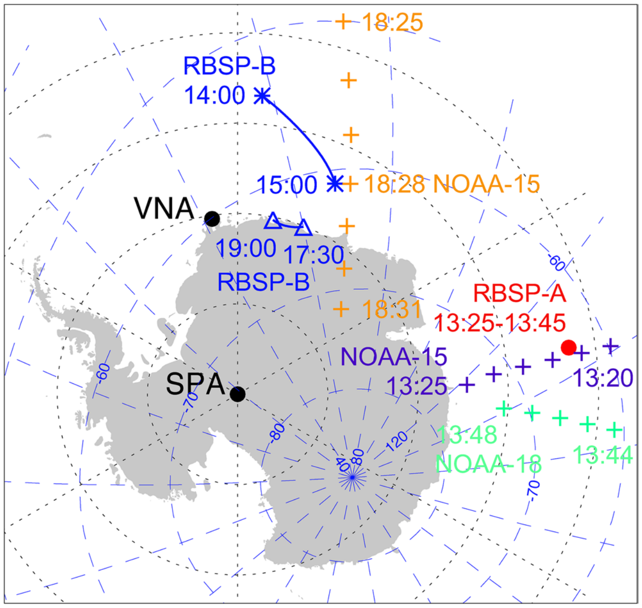

Figure 3. Map of Antarctica with Neumayer Station (VNA) and the magnetic footprint of the spacecraft tracks shown.

A more detailed view of spatiotemporal changes in PSD as a function of the first adiabatic invariant, μ and the second adiabatic invariant, K for different L^* values is presented in Figure 6. To make it easier to discern the PSD changes, these figures show the PSD ratio of "preevent pass" to "event pass" (PSD_{Pre}/PSD_{During}) and to "postevent pass" (PSD_{Pre}/PSD_{Post}) in the $\mu - K$ space for different L^* values as observed by Spacecraft A and B. The time ranges that we define as "preevent," "during," and "postevent" were determined by their orbit to include a complete range of L^*'s (i.e., from perigee to apogee or vice versa). Thus, those time ranges are as following: 08:45–13:13 UT, 13:13–17:41 UT, and 17:41–22:09 UT for Spacecraft A; 08:34–13:02 UT, 13:02–17:29 UT, and 17:29–21:57 UT for Spacecraft B. The ion concentration ratio, n_H: n_{He}: n_O = 0.93: 0.04: 0.03, was obtained using the same method described in (Min et al., 2015) in which ion concentrations are inferred from the cold plasma dispersion relation with the two cutoff frequencies of each wave band of observed wave spectra.

We chose wave frequencies 0.29 Hz and 0.9 Hz based on the Van Allen Probe-A observations, corresponding to the minimum resonant energies $E_\parallel = 5.0$ MeV (solid magenta curve) and $E_\parallel = 0.9$ MeV (dashed magenta curve), respectively. The dashed green curve corresponds to the constant total energy $E = 0.9$ MeV. The decreases in PSDs of electrons took place mostly below the resonance curve corresponding to the upper bound of the dropout energy, $E_\parallel = 5.0$ MeV and above the curve corresponding to

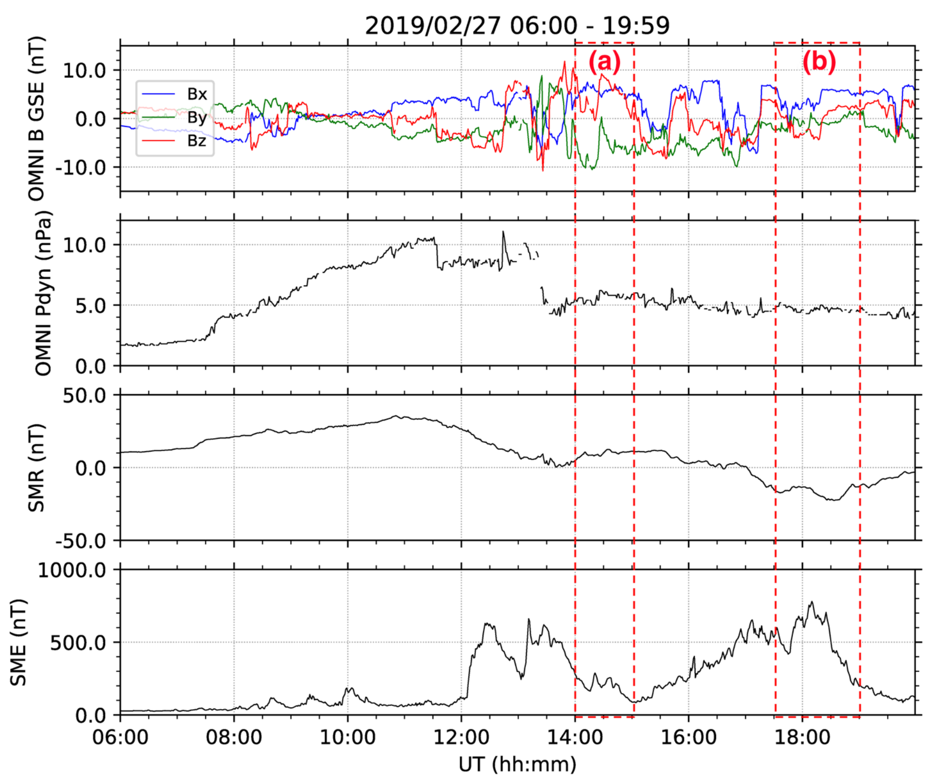

Figure 4. OMNI data showing IMF orientation (top panel) and solar wind dynamic pressure (second panel), SuperMAG ring current index (SMR, third panel), and SuperMAG auroral electrojet index (SME, bottom panel) on February 27, 2019. The red rectangles (a) and (b) indicate the time periods when the EMIC wave events were observed by Spacecraft A and B, respectively. EMIC, electromagnetic ion cyclotron.

10.1029/2020JA028503

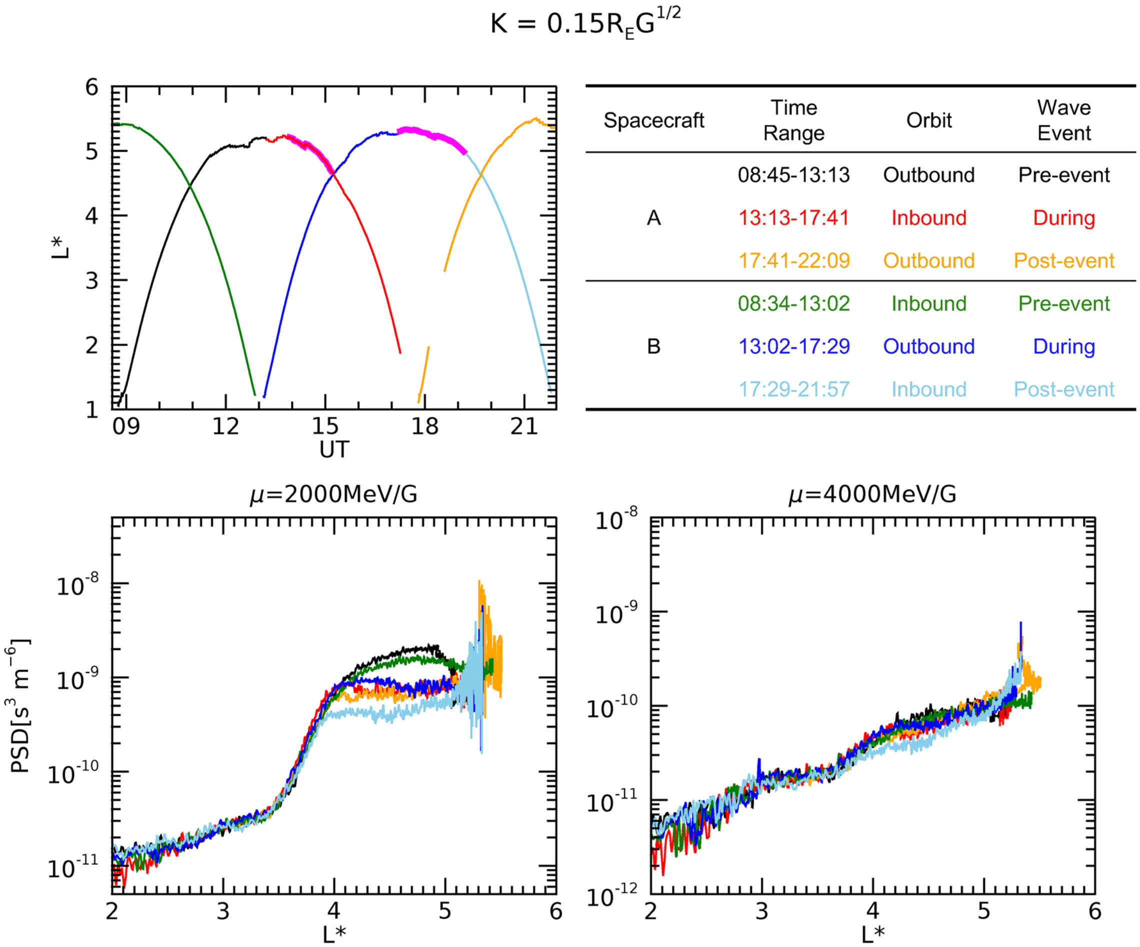

Figure 5. The temporal progression of phase space densities (PSDs) and their distributions in L^*-shell values for Spacecraft A and B. Top: L^*-shell changes of each spacecraft. The thick magenta traces indicate the times when the EMIC waves were observed by Spacecraft A and B, respectively. Bottom: PSD versus L^* for two different first adiabatic invariants, $\mu = 2{,}000$ MeV/G (left) and 4,000 MeV/G (right). The second adiabatic invariant, $K = 0.15\ R_E G^{1/2}$ for all cases.

the lower bound of the dropout energy, $E = 0.9$ MeV. The electron dropout is more dominant at $L^* = 4.5$ (Spacecraft A) and at $L^* = 4.5$–5.0 (Spacecraft B). The PSD observations clearly suggest localized (in L^*'s) electron dropout events associated with EMIC waves.

The resonance curves were calculated from the relativistic resonance condition for the parallel EMIC waves (e.g., Silin et al., 2011; Summers et al., 1998) and transformed to adiabatic coordinates (see, e.g., Boyd et al., 2014). We note that, unlike for the constant total energy curve (green curve), all energies (parallel, perpendicular and total) vary along the resonance curves (magenta curve). The curves in each panel correspond to the resonance at $L^* = 4.5$ where the waves were observed. Thus, these curves may not be meaningful at smaller L^*'s although they might be used to identify the region where PSD changes would be expected to be observed if there were waves at these L^*'s. In addition, since the pitch angle decreases with increasing K along constant energy curves, one can notice that the PSD changes at lower pitch angles (larger K) were more significant than those at larger pitch angles (smaller K) as shown in Figure 6 (at $L^* = 4.5$, in particular).

Figure 7 presents proton data during four NOAA spacecraft passes near the geomagnetic footprint of Van Allen Probes before and during the electron dropout event associated with the EMIC waves. The green rectangles denote the approximate time ranges during the conjunction flight near the footprint of Van Allen Probes. See the map in Figure 3 for locations of the spacecraft footprints. The lower energy channels (top three panels in the figure, 39, 115, and 332 keV, respectively) show increases in precipitating proton

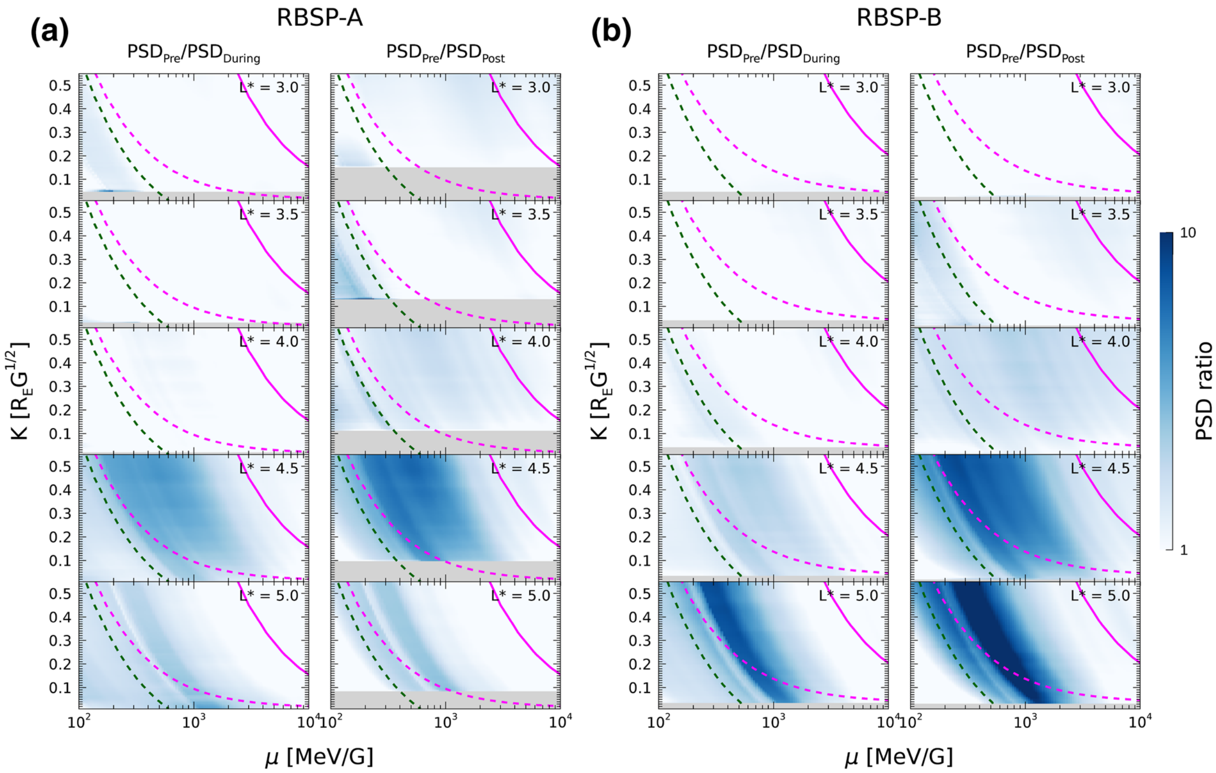

Figure 6. The PSD ratio of "pre-event pass" to "event pass" (PSD_{Pre}/PSD_{During}) and to "post-event pass" (PSD_{Pre}/PSD_{Post}) in the μ–K space for different L^* values, estimated from the spacecraft A (panel a) and spacecraft B (panel b) observations. The solid and dashed magenta lines represent resonance μ–K curves corresponding to the minimum resonant energies, $E_{\parallel} = 5.0$ and 0.9 MeV, respectively at $L^* = 4.5$. The dashed green lines represent μ–K curves of the constant total energy $E = 0.9$ MeV at $L^* = 4.5$.

flux (black traces), which are typically considered to be an indicator of the interaction of the ring current/plasma sheet protons with EMIC waves (e.g., Engebretson et al., 2015; Miyoshi et al., 2008; Yahnin & Yahnina, 2007). The highest proton energy channel (>6,174 keV, the bottom panels of the figure) of the spacecraft is often used as a proxy measurement of relativistic electrons. The first column shows NOAA-15 data before the dropout (13:20–13:30 UT), in which there is no clear precipitating particle flux (black traces, 0° telescopes). The middle and last columns present NOAA-18 and NOAA-15 data during the dropout event, displaying enhancement of precipitating relativistic electron flux. There were no further clear observations of precipitating flux enhancement during the next NOAA spacecraft passes (figures not shown here).

4. Discussion and Summary

This study presents direct evidence of radiation belt electron dropout due to EMIC waves as observed by the Van Allen Probes spacecraft, a mission that has been providing invaluable data for the study of radiation belt and ring current dynamics. It is well known that EMIC waves play a critical role in scattering radiation belt electrons from a number of theoretical and modeling studies quantifying pitch-angle scattering mechanisms due to EMIC waves (as in the references listed in Section 1). Observations of such an interaction are, however, still rare, given the limited spatiotemporal coverage of space-borne instrumentation. The event in this study presents a well-defined correspondence between EMIC wave occurrence and relativistic electron dropout as seen in PSD following ring current injection thanks to the confluence of multipoint data sets.

The injection and EMIC wave events in this paper occurred at $L = {\sim}5$–6 near the dusk sector, similar to the previous observations (e.g., L. W. Blum et al., 2015; Remya et al., 2018). It has been statistically shown that with higher auroral activity (i.e., higher AE index), the wave occurrence favors the afternoon sector (Saikin et al., 2016). This is mainly related to injected ring current ions interacting with the cold plasmaspheric

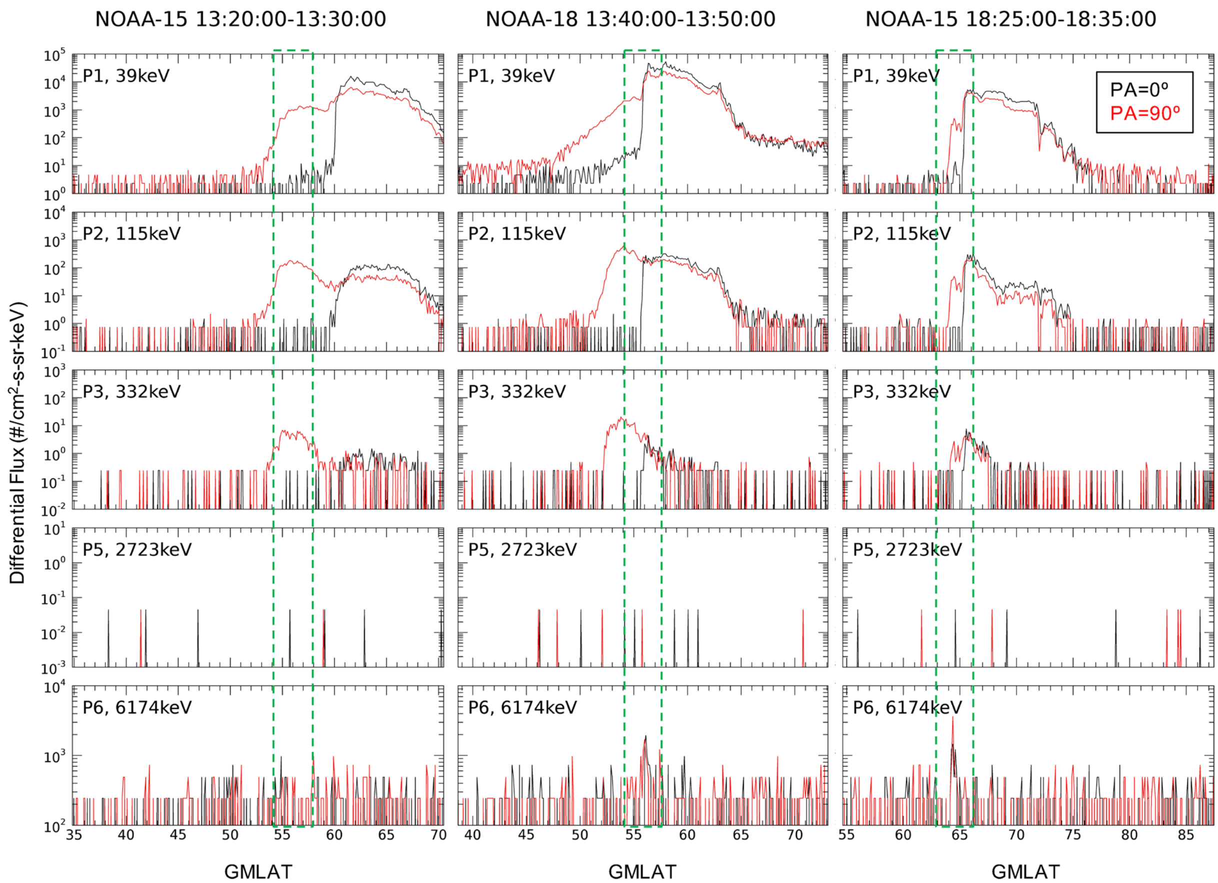

Figure 7. NOAA spacecraft observations of proton fluxes before (first column, 13:20–13:30 UT) and during (middle and last columns) the EMIC wave event observed by Van Allen Probes near the footprint. The black and red traces indicate precipitating (0°) and trapped (90°) particle flux, respectively. The green dashed rectangles denote the approximate time ranges during the conjunction flight near the footprint of Van Allen Probes before and during the dropout. EMIC, electromagnetic ion cyclotron.

population, thus lowering the EMIC instability threshold (e.g., Halford et al., 2015; Kozyra et al., 1984). Recent Van Allen Probes studies by Remya et al. (2018, 2020) showed EMIC wave events triggered by ion injection during isolated substorms with no influence from geomagnetic storms or enhancements in solar wind dynamic pressure, suggesting that an associated decrease in the geomagnetic field and enhanced temperature anisotropy provide free energy for wave generation. The EMIC waves in our study also occurred after the solar wind dynamic pressure change became stable (Figure 4). The ground magnetometer data (Figure 2) indicate that the onset of the wave activity was at ∼13 UT, accompanied by the decrease in solar wind dynamic pressure and enhanced auroral activity (Figure 4), perhaps tied to ion injection.

It is apparent that the electron dropout, seen as decreases in PSD, was associated with the EMIC waves which began at ∼13 UT (supported by the ground data) as shown in Figure 5. It is, however, still challenging to clearly identify the cause of dropout as various loss mechanisms have been proposed and either one or combination of those can contribute to loss: outward adiabatic transport (e.g., H.-J. Kim & Chan, 1997; X. Li et al., 1997), outward radial diffusion (e.g., Shprits et al., 2006), magnetopause shadowing (e.g., Turner et al., 2012, 2013; Xiang et al., 2017), and pitch-angle scattering and precipitation due to resonant interaction with plasma waves (chorus, hiss, and EMIC) (e.g., Miyoshi et al., 2008; Summers & Thorne, 2003; Turner et al., 2014; Usanova et al., 2014). Nevertheless, the events in our study provide evidence to support the idea of the dropout due to the EMIC waves, ruling out the other mechanisms because (1) the PSD decreases were seen in a limited L^* range of 4–5 (in particular, Spacecraft A observed more dominant PSD decreases near $L^* = 4.5$ than higher L^*'s; (2) the PSD decreases are energy-dependent (μ and K); (3) the μ and K profile follows the estimated energy range (1.2–3.9 MeV, Figures 6a and 6b); (4) no clear chorus waves and hiss were observed (figure not shown here); (5) last closed drift shells and magnetopause standoff positions obtained by the Tsyganenko model indicated no clear magnetopause shadowing effect during the event period (figure not shown here); (6) precipitation of relativistic electrons was observed by multiple NOAA spacecraft passing near the magnetic footprint; (7) there was persistent Pc1 wave activity over the course of the dropout event as observed by the ground magnetometer. In fact, there are recent reports of Van Allen Probes observations of EMIC wave-induced radiation belt electron dropout (e.g., L. W. Blum et al., 2020; Engebretson et al., 2015, 2018; Sigsbee et al., 2016; Xiang et al., 2017; Zhang et al., 2016). Our study provides a more direct and comprehensive view of EMIC wave-induced dropout event.

We summarize our study as follows:

1. EMIC waves were observed simultaneously in space (Van Allen Probes) and on the ground
2. Van Allen Probes particle data show that the wave event was associated with a particle injection
3. PSDs were investigated to reveal that there was a significant energy-dependent relativistic electron dropout over a limited *L*-shell range of 4–5 during and after the EMIC wave event
4. NOAA spacecraft data show relativistic electron precipitation during the dropout event

Acknowledgments

The work at the New Jersey Institute of Technology (NJIT) was supported by NSF under grant AGS-1602560 and the NASA Van Allen Probes RBSPICE instrument project, as supported by JHU/APL Subcontract No. 131803 to NJIT under NASA Prime Contract No. NNN06AA01C. The authors acknowledge support as follows: Q. Schiller, NASA grant 80NSSC20K0082; M. J. Engebretson, NSF grants PLR-1341493 and AGS-1651263; I. Kuzichev, NSF Grant AGS-1502923; K.-H. Kim, the Basic Science Research Program through National Research Foundation of Korea under grant NRF-2019R1F1A1055444; M. R. Lessard, NSF grant ANT-1745041; and D.-Y. Lee, the N ational Research Foundation of Korea under grant NRF-2019R1A2C1003140. The authors would like to thank the Van Allen Probes teams (EMFISIS, ECT, RBSPICE) for providing data utilized in this study. Processing and analysis of the HOPE, MagEIS, and REPT data were supported by the Radiation Belt Storm Probes-Energetic Particle, Composition, and Thermal Plasma (RBSP-ECT) investigation funded under NASA's Prime contract no. NAS5-01072. The fluxgate magnetometer data from Neumayer Station (VNA) are provided by Alfred Wegener Institute (AWI), Bremerhaven, Germany, and GFZ, Potsdam, Germany through https://intermagnet.org/. The MICA-S induction-coil magnetometer data from Neumayer Station (VNA) are provided by Kyung Hee University (lead institute, Korea), the University of New Hampshire (UNH), NJIT, AWI, and GFZ through the UNH induction-coil data repository at http://mirl.sr.unh.edu/. The authors gratefully acknowledge the SuperMAG collaborators (http://supermag.jhuapl.edu/info/?page=acknowledgement) for providing SuperMAG data. The authors also gratefully acknowledge use of NASA/GSFC's Space Physics Data Facility's OMNIWeb, SSCweb, and CDAWeb data.

Data Availability Statement

All Van Allen Probes data are publicly available on the following websites: http://www.RBSP-ect.lanl.gov/ (ECT), https://emfisis.physics.uiowa.edu/data/index (EMFISIS), and http://rbspice.ftecs.com/Data.html (RBSPICE). NOAA POES particle data are publicly available at https://www.ngdc.noaa.gov/stp/satellite/poes/dataaccess.html.

References

Albert, J. M., & Bortnik, J. (2009). Nonlinear interaction of radiation belt electrons with electromagnetic ion cyclotron waves. *Geophysical Research Letters*, *36*, L12110. https://doi.org/10.1029/2009GL038904

Allen, R. C., Zhang, J.-C., Kistler, L. M., Spence, H. E., Lin, R.-L., Klecker, B., et al. (2015). A statistical study of EMIC waves observed by cluster: 1. Wave properties. *Journal of Geophysical Research: Space Physics*, *120*(7), 5574–5592. https://doi.org/10.1002/2015JA021333

Allison, H., & Shprits, Y. (2020). Local heating of radiation belt electrons to ultra-relativistic energies. *Nature Communications*, *11*, 4533. https://doi.org/10.1038/s41467-020-18053-z

Anderson, B. J., Denton, R. E., Ho, G., Hamilton, D. C., Fuselier, S. A., & Strangeway, R. J. (1996). Observational test of local proton cyclotron instability in the earth's magnetosphere. *Journal of Geophysical Research*, *101*(A10), 21527–21543. https://doi.org/10.1029/96JA01251

Anderson, B. J., Erlandson, R. E., & Zanetti, L. J. (1992). A statistical study of pc 1–2 magnetic pulsations in the equatorial magnetosphere: 1. Equatorial occurrence distributions. *Journal of Geophysical Research*, *97*(A3), 3075–3088. https://doi.org/10.1029/91JA02706

Anderson, B. J., & Hamilton, D. C. (1993). Electromagnetic ion cyclotron waves stimulated by modest magnetospheric compressions. *Journal of Geophysical Research*, *98*(A7), 11369–11382. https://doi.org/10.1029/93JA00605

Arnoldy, R. L., Lewis, Jr., P. B., & Cahill, Jr., L. J. (1979). Polarization of Pc 1 and IPDP pulsations correlated with particle precipitation. *Journal of Geophysical Research*, *84*(A12), 7091–7098. https://doi.org/10.1029/JA084iA12p07091

Baker, D. N., Kanekal, S., Hoxie, V., Batiste, S., Bolton, M., Li, X., et al. (2013). The relativistic electron-proton telescope (REPT) instrument on board the radiation belt storm probes (RBSP) spacecraft: Characterization of earth's radiation belt high-energy particle populations. *Space Science Reviews*, *179*(1–4), 337–381.

Blake, J., Carranza, P., Claudepierre, S., Clemmons, J., Crain, W., Dotan, Y., et al. (2013). The magnetic electron ion spectrometer (MagEIS) instruments aboard the radiation belt storm probes (RBSP) spacecraft. In Fox, N., & Burch, J. L. (Eds.), *The Van Allen Probes Mission* (pp. 383–421). Boston, MA: Springer. https://doi.org/10.1007/978-1-4899-7433-4_12

Blum, L. W., Remya, B., Denton, M. H., & Schiller, Q. (2020). Persistent emic wave activity across the nightside inner magnetosphere. *Geophysical Research Letters*, *47*(6), e2020GL087009. https://doi.org/10.1029/2020GL087009

Blum, L., Artemyev, A., Agapitov, O., Mourenas, D., Boardsen, S., & Schiller, Q. (2019). Emic wave-driven bounce resonance scattering of energetic electrons in the inner magnetosphere. *Journal of Geophysical Research: Space Physics*, *124*(4), 2484–2496. https://doi.org/10.1029/2018JA026427

Blum, L. W., Halford, A., Millan, R., Bonnell, J. W., Goldstein, J., Usanova, M., et al. (2015). Observations of coincident emic wave activity and duskside energetic electron precipitation on 18–19 January 2013. *Geophysical Research Letters*, *42*(14), 5727–5735. https://doi.org/10.1002/2015GL065245

Borovsky, J. E., & Denton, M. H. (2009). Electron loss rates from the outer radiation belt caused by the filling of the outer plasmasphere: The calm before the storm. *Journal of Geophysical Research*, *114*, A11203. https://doi.org/10.1029/2009JA014063

Boyd, A. J., Spence, H. E., Claudepierre, S. G., Fennell, J. F., Blake, J. B., Baker, D. N., et al. (2014). Quantifying the radiation belt seed population in the 17 March 2013 electron acceleration event. *Geophysical Research Letters*, *41*(7), 2275–2281. https://doi.org/10.1002/2014GL059626

Capannolo, L., Li, W., Ma, Q., Chen, L., Shen, X.-C., Spence, H. E., et al. (2019). Direct observation of subrelativistic electron precipitation potentially driven by EMIC waves. *Geophysical Research Letters*, *46*(22), 12711–12721. https://doi.org/10.1029/2019GL084202

Capannolo, L., Li, W., Ma, Q., Shen, X.-C., Zhang, X.-J., Redmon, R. J., et al. (2019). Energetic electron precipitation: Multievent analysis of its spatial extent during EMIC wave activity. *Journal of Geophysical Research: Space Physics*, *124*(4), 2466–2483. https://doi.org/10.1029/2018JA026291

Chen, Y., Friedel, R. H. W., Reeves, G. D., Onsager, T. G., & Thomsen, M. F. (2005). Multisatellite determination of the relativistic electron phase space density at geosynchronous orbit: Methodology and results during geomagnetically quiet times. *Journal of Geophysical Research*, *110*, A10210. https://doi.org/10.1029/2004JA010895

Chen, L., Thorne, R. M., & Horne, R. B. (2009). Simulation of EMIC wave excitation in a model magnetosphere including structured high-density plumes. *Journal of Geophysical Research*, *114*, A07221. https://doi.org/10.1029/2004JA010895

Cho, J.-H., Lee, D.-Y., Noh, S.-J., Shin, D.-K., Hwang, J., Kim, K.-C., et al. (2016). Van Allen Probes observations of electromagnetic ion cyclotron waves triggered by enhanced solar wind dynamic pressure. *Journal of Geophysical Research: Space Physics*, *121*(10), 9771–9793. https://doi.org/10.1002/2016JA022841

Clausen, L. B. N., Baker, J. B. H., Ruohoniemi, J. M., & Singer, H. J. (2011). Emic waves observed at geosynchronous orbit during solar minimum: Statistics and excitation. *Journal of Geophysical Research*, *116*, A10205. https://doi.org/10.1029/2011JA016823

Denton, R. E., Ofman, L., Shprits, Y. Y., Bortnik, J., Millan, R. M., Rodger, C. J., et al. (2019). Pitch angle scattering of sub-MeV relativistic electrons by electromagnetic ion cyclotron waves. *Journal of Geophysical Research: Space Physics*, *124*(7), 5610–5626. https://doi.org/10.1029/2018JA026384

Engebretson, M. J., Peterson, W. K., Posch, J. L., Klatt, M. R., Anderson, B. J., Russell, C. T., et al. (2002). Observations of two types of Pc 1–2 pulsations in the outer dayside magnetosphere. *Journal of Geophysical Research*, *107*, 1451. https://doi.org/10.1029/2001JA000198

Engebretson, M. J., Posch, J. L., Braun, D. J., Li, W., Ma, Q., Kellerman, A. C., et al. (2018). EMIC wave events during the four GEM QARBM challenge intervals. *Journal of Geophysical Research: Space Physics*, *123*(8), 6394–6423. https://doi.org/10.1029/2018JA025505

Engebretson, M. J., Posch, J. L., Wygant, J. R., Kletzing, C. A., Lessard, M. R., Huang, C.-L., et al. (2015). Van Allen Probes, NOAA, GOES, and ground observations of an intense EMIC wave event extending over 12 h in magnetic local time. *Journal of Geophysical Research: Space Physics*, *120*(7), 5465–5488. https://doi.org/10.1002/2015JA021227

Erlandson, R. E., & Ukhorskiy, A. J. (2001). Observations of electromagnetic ion cyclotron waves during geomagnetic storms: Wave occurrence and pitch angle scattering. *Journal of Geophysical Research*, *106*(A3), 3883–3895. https://doi.org/10.1029/2000JA000083

Foster, J. C., Wygant, J. R., Hudson, M. K., Boyd, A. J., Baker, D. N., Erickson, P. J., & Spence, H. E. (2015). Shock-induced prompt relativistic electron acceleration in the inner magnetosphere. *Journal of Geophysical Research: Space Physics*, *120*(3), 1661–1674. https://doi.org/10.1002/2014JA020642

Fraser, B. J., Grew, R. S., Morley, S. K., Green, J. C., Singer, H. J., Loto'aniu, T. M., & Thomsen, M. F. (2010). Storm time observations of electromagnetic ion cyclotron waves at geosynchronous orbit: Goes results. *Journal of Geophysical Research*, *115*, A05208. https://doi.org/10.1029/2009JA014516

Funsten, H., Skoug, R., Guthrie, A., MacDonald, E., Baldonado, J., Harper, R., et al. (2013). Helium, oxygen, proton, and electron (HOPE) mass spectrometer for the radiation belt storm probes mission. *Space Science Reviews*, *179*(1–4), 423–484.

Galand, M., & Evans, D. (2000). *Radiation damage of the proton MEPED detector on POES (TIROS/NOAA) satellites*, (NOAA Technical Report). Boulder, CO: National Oceanic and Atmospheric Administration.

Gjerloev, J. W. (2012). The supermag data processing technique. *Journal of Geophysical Research*, *117*, A09213. https://doi.org/10.1029/2012JA017683

Halford, A. J., Fraser, B. J., & Morley, S. K. (2010). EMIC wave activity during geomagnetic storm and nonstorm periods: CRRES results. *Journal of Geophysical Research*, *115*(A12). https://doi.org/10.1029/2010JA015716

Halford, A. J., Fraser, B. J., & Morley, S. K. (2015). EMIC waves and plasmaspheric and plume density: CRRES results. *Journal of Geophysical Research: Space Physics*, *120*(3), 1974–1992. https://doi.org/10.1002/2014JA020338

Hayashi, K., Yamamoto, T., Kokubun, S., Oguti, T., & Ogawa, T. (1988). Multi-station observation of IPDP micropulsations—Two-dimensional distribution and evolution of the source regions. *Journal of Geomagnetism and Geoelectricity*, *40*(5), 583–619. https://doi.org/10.5636/jgg.40.583

Johnson, J. R., & Cheng, C. Z. (1999). Can ion cyclotron waves propagate to the ground? *Geophysical Research Letters*, *26*(6), 671–674. https://doi.org/10.1029/1999GL900074

Jordanova, V. K., Albert, J., & Miyoshi, Y. (2008). Relativistic electron precipitation by emic waves from self-consistent global simulations. *Journal of Geophysical Research*, *113*, A00A10. https://doi.org/10.1029/2008JA013239

Jordanova, V. K., Farrugia, C. J., Thorne, R. M., Khazanov, G. V., Reeves, G. D., & Thomsen, M. F. (2001). Modeling ring current proton precipitation by electromagnetic ion cyclotron waves during the May 14–16, 1997, storm. *Journal of Geophysical Research*, *106*(A1), 7–22. https://doi.org/10.1029/2000JA002008

Kangas, J., Pikkarainen, T., & Olson, J. (1987). Simultaneous observations of IPDP type wave events in the evening and morning hours. *Planetary and Space Science*, *35*(6), 827–832. https://doi.org/10.1016/0032-0633(87)90044-4

Katsavrias, C., Daglis, I. A., & Li, W. (2019). On the statistics of acceleration and loss of relativistic electrons in the outer radiation belt: A superposed epoch analysis. *Journal of Geophysical Research: Space Physics*, *124*(4), 2755–2768. https://doi.org/10.1029/2019JA026569

Keika, K., Takahashi, K., Ukhorskiy, A. Y., & Miyoshi, Y. (2013). Global characteristics of electromagnetic ion cyclotron waves: Occurrence rate and its storm dependence. *Journal of Geophysical Research: Space Physics*, *118*(7), 4135–4150. https://doi.org/10.1002/jgra.50385

Kennel, C. F., & Petschek, H. E. (1966). Limit on stably trapped particle fluxes. *Journal of Geophysical Research*, *71*(1), 1–28. https://doi.org/10.1029/JZ071i001p00001

Khazanov, G. V., & Gamayunov, K. V. (2007). Effect of electromagnetic ion cyclotron wave normal angle distribution on relativistic electron scattering in outer radiation belt. *Journal of Geophysical Research*, *112*, A10209. https://doi.org/10.1029/2007JA012282

Kim, H.-J., & Chan, A. A. (1997). Fully adiabatic changes in storm time relativistic electron fluxes. *Journal of Geophysical Research*, *102*(A10), 22107–22116. https://doi.org/10.1029/97JA01814

Kim, H., Clauer, C. R., Gerrard, A. J., Engebretson, M. J., Hartinger, M. D., Lessard, M. R., et al. (2017). Conjugate observations of electromagnetic ion cyclotron waves associated with traveling convection vortex events. *Journal of Geophysical Research: Space Physics*, *122*(7), 7336–7352. https://doi.org/10.1002/2017JA024108

Kim, E.-H., & Johnson, J. R. (2016). Full-wave modeling of EMIC waves near the He+ gyrofrequency. *Geophysical Research Letters*, *43*(1), 13–21. https://doi.org/10.1002/2015GL066978

Kim, H., Lessard, M. R., Engebretson, M. J., & Young, M. A. (2011). Statistical study of Pc1–2 wave propagation characteristics in the high-latitude ionospheric waveguide. *Journal of Geophysical Research*, *116*, A07227. https://doi.org/10.1029/2010JA016355

Kim, K.-H., Park, J.-S., Omura, Y., Shiokawa, K., Lee, D.-H., Kim, G.-J., et al. (2016). Spectral characteristics of steady quiet-time EMIC waves observed at geosynchronous orbit. *Journal of Geophysical Research: Space Physics*, *121*(9), 8640–8660. https://doi.org/10.1002/2016JA022957

King, J. H., & Papitashvili, N. E. (2005). Solar wind spatial scales in and comparisons of hourly wind and ace plasma and magnetic field data. *Journal of Geophysical Research*, *110*, A02104. https://doi.org/10.1029/2004JA010649

Kletzing, C. A., Kurth, W. S., Acuna, M., MacDowall, R. J., Torbert, R. B., Averkamp, T., et al. (2013). The Electric and Magnetic Field Instrument Suite and Integrated Science (EMFISIS) on RBSP. *Space Science Reviews*, *179*(1–4), 127–181. https://doi.org/10.1007/s11214-013-9993-6

Kozyra, J. U., Jordanova, V. K., Home, R. B., & Thorne, R. M. (1997). Modeling of the contribution of electromagnetic ion cyclotron (EMIC) waves to stormtime ring current erosion. In Tsurutani, B. T., Gonzalez, W. D., Kamide, Y., & Arballo, J. K. (Eds.), *Magnetic storms* (pp. 187–202). Washington, DC: American Geophysical Union. https://doi.org/10.1029/GM098p0187

Kozyra, J. U., Cravens, T. E., Nagy, A. F., Fontheim, E. G., & Ong, R. S. B. (1984). Effects of energetic heavy ions on electromagnetic ion cyclotron wave generation in the plasmapause region. *Journal of Geophysical Research*, *89*(A4), 2217–2233. https://doi.org/10.1029/JA089iA04p02217

Lee, D.-Y., Kim, K.-C., & Choi, C.-R. (2020). Nonlinear scattering of 90° pitch angle electrons in the outer radiation belt by large-amplitude emic waves. *Geophysical Research Letters*, *47*(4), e2019GL086738. https://doi.org/10.1029/2019GL086738

Lessard, M. R., Paulson, K., Spence, H. E., Weaver, C., Engebretson, M. J., Millan, R., et al. (2019). Generation of EMIC waves and effects on particle precipitation during a solar wind pressure intensification with Bz>0. *Journal of Geophysical Research: Space Physics*, *124*(6), 4492–4508. https://doi.org/10.1029/2019JA026477

Li, X., Baker, D. N., Temerin, M., Cayton, T. E., Reeves, E. G. D., Christensen, R. A., et al. (1997). Multisatellite observations of the outer zone electron variation during the November 3–4, 1993, magnetic storm. *Journal of Geophysical Research*, *102*(A7), 14123–14140. https://doi.org/10.1029/97JA01101

Li, Z., Millan, R. M., Hudson, M. K., Woodger, L. A., Smith, D. M., Chen, Y., et al. (2014). Investigation of EMIC wave scattering as the cause for the barrel 17 January 2013 relativistic electron precipitation event: A quantitative comparison of simulation with observations. *Geophysical Research Letters*, *41*(24), 8722–8729. https://doi.org/10.1002/2014GL062273

Lin, R.-L., Zhang, J.-C., Allen, R. C., Kistler, L., Mouikis, C., Gong, J.-C., et al. (2014). Testing linear theory of EMIC waves in the inner magnetosphere: Cluster observations. *Journal of Geophysical Research: Space Physics*, *119*(2), 1004–1027. https://doi.org/10.1002/2013JA019541

Loto'aniu, T. M., Thorne, R. M., Fraser, B. J., & Summers, D. (2006). Estimating relativistic electron pitch angle scattering rates using properties of the electromagnetic ion cyclotron wave spectrum. *Journal of Geophysical Research*, *111*(A4). https://doi.org/10.1029/2005JA011452

Lyons, L. R., & Thorne, R. M. (1972). Parasitic pitch angle diffusion of radiation belt particles by ion cyclotron waves. *Journal of Geophysical Research*, *77*(28), 5608–5616. https://doi.org/10.1029/JA077i028p05608

Mann, I. R., Usanova, M. E., Murphy, K., Robertson, M. T., Milling, D. K., Kale, A., et al. (2014). Spatial localization and ducting of EMIC waves: Van Allen Probes and ground-based observations. *Geophysical Research Letters*, *41*(3), 785–792. https://doi.org/10.1002/2013GL058581

Meredith, N. P., Thorne, R. M., Horne, R. B., Summers, D., Fraser, B. J., & Anderson, R. R. (2003). Statistical analysis of relativistic electron energies for cyclotron resonance with emic waves observed on CRRES. *Journal of Geophysical Research*, *108*, 1250. https://doi.org/10.1029/2002JA009700

Min, K., Lee, J., Keika, K., & Li, W. (2012). Global distribution of emic waves derived from THEMIS observations. *Journal of Geophysical Research*, *117*, A05219. https://doi.org/10.1029/2012JA017515

Min, K., Liu, K., Bonnell, J. W., Breneman, A. W., Denton, R. E., Funsten, H. O., et al. (2015). Study of EMIC wave excitation using direct ion measurements. *Journal of Geophysical Research: Space Physics*, *120*(4), 2702–2719. https://doi.org/10.1002/2014JA020717

Mitchell, D. G., Lanzerotti, L. J., Kim, C. K., Stokes, M., Ho, G., Cooper, S., et al. (2013). Radiation Belt Storm Probes Ion Composition Experiment (RBSPICE). *Space Science Reviews*, *179*(1–4), 263–308. https://doi.org/10.1007/s11214-013-9965-x

Miyoshi, Y., Sakaguchi, K., Shiokawa, K., Evans, D., Albert, J., Connors, M., & Jordanova, V. (2008). Precipitation of radiation belt electrons by EMIC waves, observed from ground and space. *Geophysical Research Letters*, *35*(23). https://doi.org/10.1029/2008GL035727

Morley, S. K., Ables, S. T., Sciffer, M. D., & Fraser, B. J. (2009). Multipoint observations of Pc1-2 waves in the afternoon sector. *Journal of Geophysical Research*, *114*, A09205. https://doi.org/10.1029/2009JA014162

Newell, P. T., & Gjerloev, J. W. (2011). Evaluation of supermag auroral electrojet indices as indicators of substorms and auroral power. *Journal of Geophysical Research*, *116*, A12211. https://doi.org/10.1029/2011JA016779

Newell, P. T., & Gjerloev, J. W. (2012). Supermag-based partial ring current indices. *Journal of Geophysical Research*, *117*, A05215. https://doi.org/10.1029/2012JA017586

Noh, S.-J., Lee, D.-Y., Choi, C.-R., Kim, H., & Skoug, R. (2018). Test of ion cyclotron resonance instability using proton distributions obtained from Van Allen Probe-a observations. *Journal of Geophysical Research: Space Physics*, *123*(8), 6591–6610. https://doi.org/10.1029/2018JA025385

Onsager, T. G., Chan, A. A., Fei, Y., Elkington, S. R., Green, J. C., & Singer, H. J. (2004). The radial gradient of relativistic electrons at geosynchronous orbit. *Journal of Geophysical Research*, *109*, A05221. https://doi.org/10.1029/2003JA010368

Park, J.-S., Kim, K.-H., Shiokawa, K., Lee, D.-H., Lee, E., Kwon, H.-J., et al. (2016). Emic waves observed at geosynchronous orbit under quiet geomagnetic conditions (*Kp*<=1). *Journal of Geophysical Research: Space Physics*, *121*(2), 1377–1390. https://doi.org/10.1002/2015JA021968

Qin, M., Hudson, M., Millan, R., Woodger, L., & Shen, X. (2020). Statistical dependence of emic wave scattering on wave and plasma parameters. *Journal of Geophysical Research: Space Physics*, *125*(4), e2020JA027772. https://doi.org/10.1029/2020JA027772

Qin, M., Hudson, M., Millan, R., Woodger, L., & Shekhar, S. (2018). Statistical investigation of the efficiency of emic waves in precipitating relativistic electrons. *Journal of Geophysical Research: Space Physics*, *123*(8), 6223–6230. https://doi.org/10.1029/2018JA025419

Reeves, G. D., Spence, H. E., Henderson, M. G., Morley, S. K., Friedel, R. H. W., Funsten, H. O., et al. (2013). Electron acceleration in the heart of the Van Allen radiation belts. *Science*, *341*(6149), 991–994. Retrieved from https://science.sciencemag.org/content/341/6149/991; https://doi.org/10.1126/science.1237743

Remya, B., Sibeck, D. G., Ruohoniemi, J. M., Kunduri, B., Halford, A. J., Reeves, G. D., & Reddy, R. V. (2020). Association between emic wave occurrence and enhanced convection periods during ion injections. *Geophysical Research Letters*, *47*(3), e2019GL085676. https://doi.org/10.1029/2019GL085676

Remya, B., Sibeck, D. G., Halford, A. J., Murphy, K. R., Reeves, G. D., Singer, H. J., et al. (2018). Ion injection triggered emic waves in the earth's magnetosphere. *Journal of Geophysical Research: Space Physics*, *123*(6), 4921–4938. https://doi.org/10.1029/2018JA025354

Roederer, J. G. (2012). Dynamics of geomagnetically trapped radiation (Vol. 2), New York, NY: Springer Science & Business Media.

Saikin, A. A., Zhang, J.-C., Allen, R. C., Smith, C. W., Kistler, L. M., Spence, H. E., et al. (2015). The occurrence and wave properties of H+-, He+-, and O+-band emic waves observed by the Van Allen Probes. *Journal of Geophysical Research: Space Physics*, *120*(9), 7477–7492. https://doi.org/10.1002/2015JA021358

Saikin, A. A., Zhang, J.-C., Smith, C. W., Spence, H. E., Torbert, R. B., & Kletzing, C. A. (2016). The dependence on geomagnetic conditions and solar wind dynamic pressure of the spatial distributions of emic waves observed by the Van Allen Probes. *Journal of Geophysical Research: Space Physics*, *121*(5), 4362–4377. https://doi.org/10.1002/2016JA022523

Shprits, Y. Y., Drozdov, A. Y., Spasojevic, M., Kellerman, A. C., Usanova, M. E., Engebretson, M. J., et al. (2016). Wave-induced loss of ultra-relativistic electrons in the Van Allen radiation belts. *Nature Communications*, *7*, 12883. https://doi.org/10.1038/ncomms12883

Shprits, Y. Y., Thorne, R. M., Friedel, R., Reeves, G. D., Fennell, J., Baker, D. N., & Kanekal, S. G. (2006). Outward radial diffusion driven by losses at magnetopause. *Journal of Geophysical Research*, *111*, A11214. https://doi.org/10.1029/2006JA011657

Sigsbee, K., Kletzing, C. A., Smith, C. W., MacDowall, R., Spence, H., Reeves, G., et al. (2016). Van Allen Probes, THEMIS, GOES, and cluster observations of EMIC waves, ULF pulsations, and an electron flux dropout. *Journal of Geophysical Research: Space Physics*, *121*(3), 1990–2008. https://doi.org/10.1002/2014JA020877

Silin, I., Mann, I. R., Sydora, R. D., Summers, D., & Mace, R. L. (2011). Warm plasma effects on electromagnetic ion cyclotron wave MeV electron interactions in the magnetosphere. *Journal of Geophysical Research*, *116*(A5). https://doi.org/10.1029/2010JA016398

Søraas, F., Lundblad, J. A., Maltseva, N. F., Troitskaia, V., & Selivanov, V. (1980). A comparison between simultaneous I.P.D.P. ground-based observations and observations of energetic protons obtained by satellites. *Planetary and Space Science*, *28*(4), 387–405. https://doi.org/10.1016/0032-0633(80)90043-4

Spasojević, M., Frey, H. U., Thomsen, M. F., Fuselier, S. A., Gary, S. P., Sandel, B. R., & Inan, U. S. (2004). The link between a detached subauroral proton arc and a plasmaspheric plume. *Geophysical Research Letters*, *31*, L04803. https://doi.org/10.1029/2003GL018389

Spence, H. E., Reeves, G. D., Baker, D. N., Blake, J. B., Bolton, M., Bourdarie, S., et al. (2013). Science goals and overview of the radiation belt storm probes (RBSP) energetic particle, composition, and thermal plasma (ECT) suite on NASA's Van Allen Probes mission. *Space Science Reviews*, *179*(1–4), 311–336. https://doi.org/10.1007/s11214-013-0007-5

Summers, D., & Thorne, R. M. (2003). Relativistic electron pitch-angle scattering by electromagnetic ion cyclotron waves during geomagnetic storms. *Journal of Geophysical Research*, *108*, 1143. https://doi.org/10.1029/2002JA009489

Summers, D., Thorne, R. M., & Xiao, F. (1998). Relativistic theory of wave-particle resonant diffusion with application to electron acceleration in the magnetosphere. *Journal of Geophysical Research*, *103*(A9), 20487–20500. https://doi.org/10.1029/98JA01740

Tetrick, S. S., Engebretson, M. J., Posch, J. L., Olson, C. N., Smith, C. W., Denton, R. E., et al. (2017). Location of intense electromagnetic ion cyclotron (EMIC) wave events relative to the plasmapause: Van Allen probes observations. *Journal of Geophysical Research: Space Physics*, *122*(4), 4064–4088. https://doi.org/10.1002/2016JA023392

Thorne, R. M. (2010). Radiation belt dynamics: The importance of wave-particle interactions. *Geophysical Research Letters*, *37*, L22107. https://doi.org/10.1029/2010GL044990

Thorne, R. M., & Kennel, C. F. (1971). Relativistic electron precipitation during magnetic storm main phase. *Journal of Geophysical Research*, *76*(19), 4446–4453. https://doi.org/10.1029/JA076i019p04446

Tsyganenko, N. A., & Sitnov, M. I. (2005). Modeling the dynamics of the inner magnetosphere during strong geomagnetic storms. *Journal of Geophysical Research*, *110*, A03208. https://doi.org/10.1029/2004JA010798

Turner, D. L., Angelopoulos, V., Li, W., Bortnik, J., Ni, B., Ma, Q., et al. (2014). Competing source and loss mechanisms due to wave-particle interactions in earth's outer radiation belt during the 30 September to 3 October 2012 geomagnetic storm. *Journal of Geophysical Research: Space Physics*, *119*(3), 1960–1979. https://doi.org/10.1002/2014JA019770

Turner, D. L., Morley, S. K., Miyoshi, Y., Ni, B., & Huang, C.-L. (2013). Outer radiation belt flux dropouts: Current understanding and unresolved questions. In Summers, D., Mann, I. R., Baker, D. N., & Schulz, M. (Eds.), *Dynamics of the earth's radiation belts and inner magnetosphere* (pp. 195–212). Washington, DC: American Geophysical Union. https://doi.org/10.1029/2012GM001310

Turner, D. L., Shprits, Y., Hartinger, M., & Angelopoulos, V. (2012). Explaining sudden losses of outer radiation belt electrons during geomagnetic storms. *Nature Physics*, *8*(3), 208–212. https://doi.org/10.1038/nphys2185

Ukhorskiy, A. Y., Shprits, Y. Y., Anderson, B. J., Takahashi, K., & Thorne, R. M. (2010). Rapid scattering of radiation belt electrons by storm-time EMIC waves. *Geophysical Research Letters*, *37*, L09101. https://doi.org/10.1029/2010GL042906

Usanova, M. E., Drozdov, A., Orlova, K., Mann, I. R., Shprits, Y., Robertson, M. T., et al. (2014). Effect of EMIC waves on relativistic and ultrarelativistic electron populations: Ground-based and Van Allen Probes observations. *Geophysical Research Letters*, *41*(5), 1375–1381. https://doi.org/10.1002/2013GL059024

Usanova, M. E., Mann, I. R., Bortnik, J., Shao, L., & Angelopoulos, V. (2012). THEMIS observations of electromagnetic ion cyclotron wave occurrence: Dependence on AE, SYMH, and solar wind dynamic pressure. *Journal of Geophysical Research*, *117*, A10218. https://doi.org/10.1029/2012JA018049

Usanova, M. E., Mann, I. R., Kale, Z. C., Rae, I. J., Sydora, R. D., Sandanger, M., et al. (2010). Conjugate ground and multisatellite observations of compression-related emic Pc1 waves and associated proton precipitation. *Journal of Geophysical Research*, *115*, A07208. https://doi.org/10.1029/2009JA014935

Usanova, M. E., Mann, I. R., Rae, I. J., Kale, Z. C., Angelopoulos, V., Bonnell, J. W., et al. (2008). Multipoint observations of magnetospheric compression-related EMIC Pc1 waves by THEMIS and CARISMA. *Geophysical Research Letters*, *35*, L17S25. https://doi.org/10.1029/2008GL034458

Wesche, C., Weller, R., König-Lango, G., Fromm, T., Eckstaller, A., Nixdorf, U., & Kohlberg, E. (2016). Neumayer III and Kohnen station in Antarctica operated by the Alfred Wegener Institute. *Journal of large-scale research facilities*, *2*(A85). https://doi.org/10.17815/jlsrf-2-152

Xiang, Z., Tu, W., Li, X., Ni, B., Morley, S. K., & Baker, D. N. (2017). Understanding the mechanisms of radiation belt dropouts observed by Van Allen Probes. *Journal of Geophysical Research: Space Physics*, *122*(10), 9858–9879. https://doi.org/10.1002/2017JA024487

Yahnina, T. A., Yahnin, A. G., Kangas, J., Manninen, J., Evans, D. S., Demekhov, A. G., et al. (2003). Energetic particle counterparts for geomagnetic pulsations of Pc1 and IPDP types. *Annales Geophysicae*, *21*(12), 2281–2292. Retrieved from https://hal.archives-ouvertes.fr/hal-00317198

Yahnin, A., & Yahnina, T. (2007). Energetic proton precipitation related to ion–cyclotron waves. *Journal of Atmospheric and Solar-Terrestrial Physics*, *69*(14), 1690–1706. Retrieved from http://www.sciencedirect.com/science/article/pii/S1364682607001885; https://doi.org/10.1016/j.jastp.2007.02.010

Yuan, Z., Deng, X., Lin, X., Pang, Y., Zhou, M., Décréau, P. M. E., et al. (2010). Link between EMIC waves in a plasmaspheric plume and a detached sub-auroral proton arc with observations of cluster and image satellites. *Geophysical Research Letters*, *37*, L07108. https://doi.org/10.1029/2010GL042711

Zhang, X.-J., Li, W., Ma, Q., Thorne, R. M., Angelopoulos, V., Bortnik, J., et al. (2016). Direct evidence for EMIC wave scattering of relativistic electrons in space. *Journal of Geophysical Research: Space Physics*, *121*(7), 6620–6631. https://doi.org/10.1002/2016JA022521